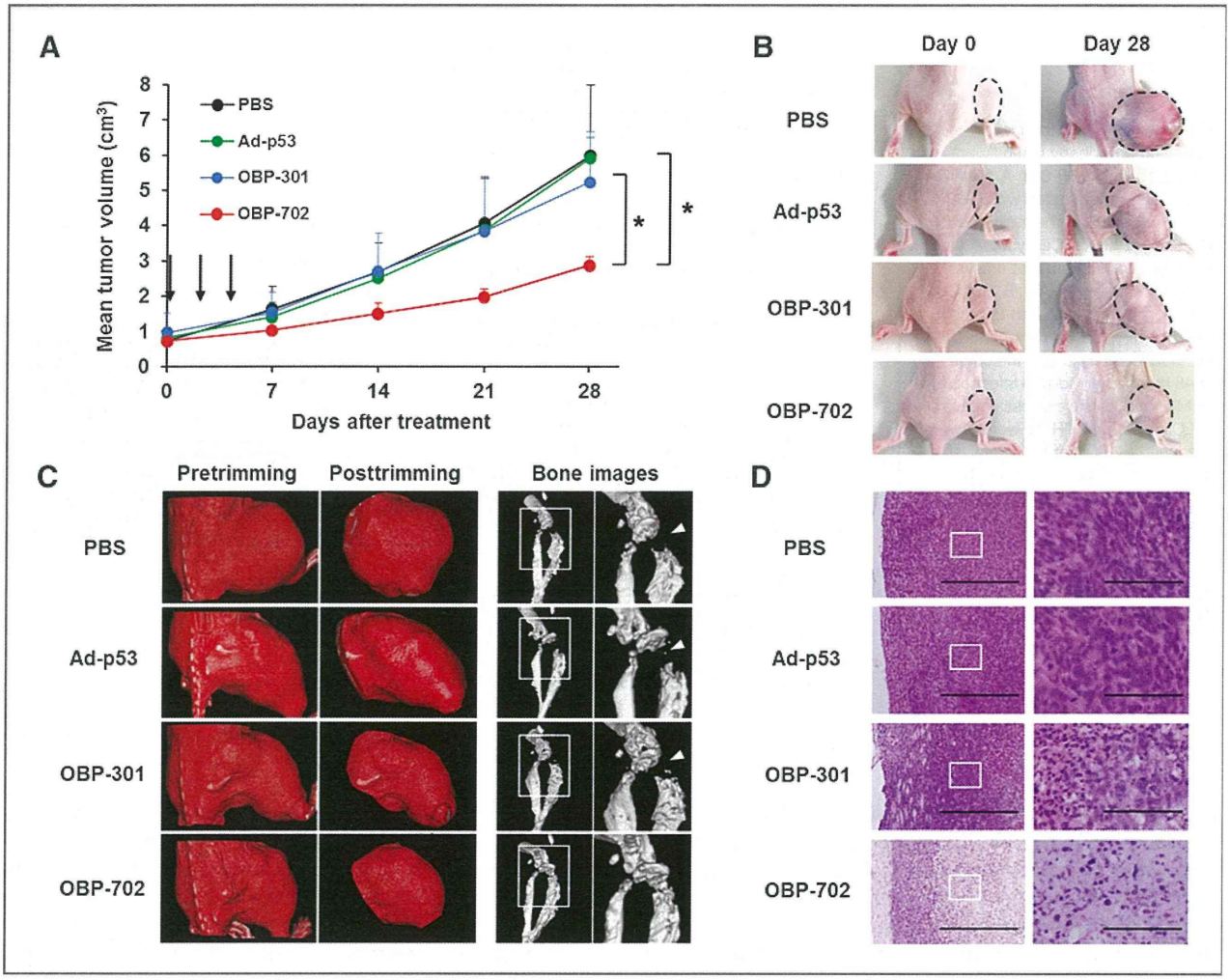

Figure 5. Antitumor effect of OBP-702 in an orthotopic MNNG/HOS osteosarcoma xenograft model. A, athymic nude mice were inoculated intratibially with MNNG/HOS cells (5×10^6 cells/site). Twenty-one days after inoculation (designated as day 0), Ad-p53, OBP-301, or OBP-702 were injected into the tumor with 1×10^8 PFUs on days 0, 2, and 4 (black arrows). PBS was used as a control. Three mice were used for each group. Each tumor volume was assessed by CT examination. Tumor growth was expressed as mean tumor volume ± SD. Statistical significance was determined by Student *t* test. *, $P < 0.05$. B, macroscopic appearance of MNNG/HOS tumors in nude mice on days 0 and 28 after treatment with PBS, Ad-p53, OBP-301, or OBP-702. Tumor masses are outlined by a dotted line. C, 3D-CT images of MNNG/HOS tumors. The tumor volumes were calculated by the image viewer (INTAGE Realia) based on 3D-CT images of tumors after trimming. The white arrowheads indicate the osteolytic areas within tumor tissues treated with PBS, Ad-p53, or OBP-301. Left side images are low magnification and right side images are high magnification of the area outlined by a white square. D, histologic analysis of the MNNG/HOS tumors. Tumor tissues were obtained on day 28 after first treatment with PBS, Ad-p53, OBP-301, or OBP-702. Paraffin-embedded sections of MNNG/HOS tumors were stained with hematoxylin and eosin solutions. There were large necrotic areas in MNNG/HOS tumors treated with OBP-702. Left side images are low magnification and right side images are high magnification of the area outlined by a white square. Left scale bars, 500 μm. Right scale bars, 100 μm.

that E2F1 enhanced Ad-p53–mediated apoptosis through p14ARF-dependent MDM2 downregulation (39) and that OBP-702 infection showed E1A-dependent MDM2 downregulation in association with apoptosis (26). Recently, E2F1 has been shown to suppress MDM2 expression by suppressing the promoter activity (40) or by inducing upregulation of *miR-25/32*, which targets MDM2 (41). Furthermore, E2F1-inducible *miR-93/106b* enhanced Ad-p53–induced apoptosis and autophagy via p21 suppression (Figs. 3D and 4B). Therefore, the cooperation between the MDM2/p53/p21 pathway and the E2F1/miRNA pathway may be involved in the induction of apoptotic and autophagic cell death in response to OBP-702.

OBP-702–mediated p53 overexpression enhanced autophagy that was induced by oncolytic adenovirus in human osteosarcoma cells. OBP-702 infection induced increased expression of DRAM and decreased expression of p62 when compared with OBP-301 (Fig. 4), suggesting that OBP-702–mediated p53 overexpression enhances autophagy through DRAM activation. We recently reported that OBP-301 induces autophagy through E1A-dependent activation of E2F1/*miR-7* pathway and subsequent suppression of EGF receptor

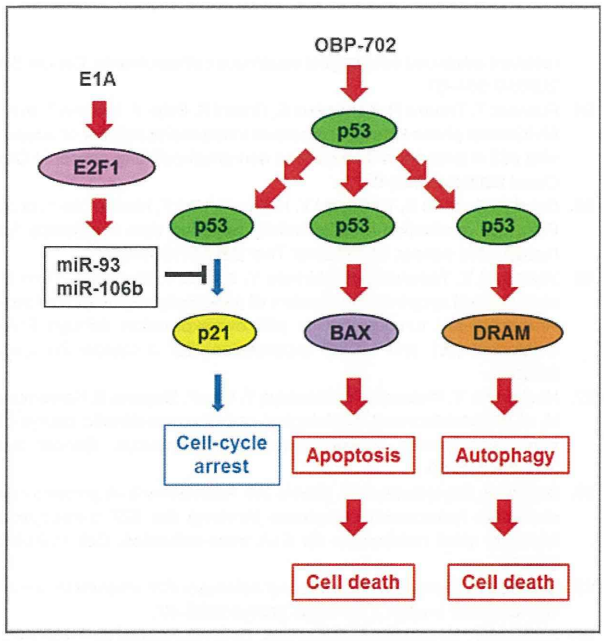

Figure 6. Outline of OBP-702–mediated induction of dual programmed cell death pathways. OBP-702 infection induces apoptosis and autophagy, leading to cell death, through p53-dependent BAX/DRAM upregulation and E1A-dependent p21 downregulation via E2F1-inducible *miR-93/106b* activation.

(EGFR; ref. 31). Restoration of p53 expression enhances the sensitivity to EGFR inhibitors in human cancer cells (42). Moreover, EGFR downregulation by transfection of specific antisense oligonucleotide promotes the differentiation status of human osteosarcoma U2OS cells (43). Thus, OBP-702 may induce differentiation as well as cell death through autophagy activation by DRAM upregulation and EGFR downregulation in human osteosarcoma cells.

The 3D-CT imaging system was a useful method to assess both tumor volume and bone destruction status in MNNG/HOS tumors. OBP-702–treated tumors were smaller and had less bone destruction than PBS-, Ad-p53-, or OBP-301–treated tumors (Fig. 5A and C). Recent reports have suggested that zoledronic acid suppresses tumor growth as well as osteolytic components in human osteosarcoma xenograft tumor models (44, 45). These results suggest that combination therapy with OBP-702 and zoledronic acid may be more effective and more protective against bone destruction in human osteosarcomas. Further study using a 3D-CT imaging system may provide important information about bone destruction status in osteosarcomas treated with OBP-702 and zoledronic acid.

Adenovirus-mediated *p53* gene therapy exerts an antitumor effect in human osteosarcoma cells (46). However, the antitumor activity of replication-deficient Ad-p53 is limited in some human osteosarcoma cells (47). Ad-p53–mediated p53 overexpression increases the sensitivity of human osteosarcoma cells to the chemotherapeutic drugs, cisplatin and doxorubicin (48). A synergistic antitumor effect between doxorubicin and roscovitine was also associated with autophagy induction in human osteosarcoma U2OS cells (49). As OBP-702 induced more profound apoptosis and autophagy than did OBP-301 or Ad-p53 (Fig. 2 and 4), combination therapy with OBP-702 and chemotherapeutic agents may be more effective than monotherapy with OBP-702. Moreover, a recent report has shown that p53-armed replication-competent oncolytic adenovirus is a safe antitumor agent in rodents and non-human primates (50). However, for clinical application of OBP-702, it must be necessary to establish the systemic delivery method and confirm the host biologic contributions in patients with cancer. Although there are some unsolved issues, the combination of p53-armed oncolytic adenovirus and chemotherapy may provide us a promising antitumor strategy against human osteosarcoma cells.

In conclusion, we clearly showed that the p53-expressing oncolytic adenovirus OBP-702 has a much stronger antitumor effect than does OBP-301. Oncolytic adenovirus-mediated *p53* gene transduction may induce dual apoptotic and autophagic cell death pathways through p53-dependent activation of cell death inducers and E1A-dependent suppression of cell death inhibitors, resulting in the enhancement of antitumor effect.

Disclosure of Potential Conflicts of Interest

Y. Urata is President & CEO of Oncolys BioPharma, Inc., the manufacturer of OBP-301 (Telomelysin). H. Tazawa and T. Fujiwara are consultants of Oncolys BioPharma, Inc. No potential conflicts of interest were disclosed by the other authors.

Authors' Contributions

Conception and design: J. Hasei, F. Uno, S. Kagawa, T. Ozaki, T. Fujiwara
Development of methodology: J. Hasei, F. Uno, S. Kagawa
Acquisition of data (provided animals, acquired and managed patients, provided facilities, etc.): J. Hasei, H. Tazawa, S. Osaki, Y. Yamakawa, A. Yoshida, T. Onishi, T. Ozaki
Analysis and interpretation of data (e.g., statistical analysis, biostatistics, computational analysis): J. Hasei, H. Tazawa, T. Fujiwara
Writing, review, and/or revision of the manuscript: J. Hasei, H. Tazawa, T. Kunisada, Y. Urata, T. Fujiwara
Administrative, technical, or material support (i.e., reporting or organizing data, constructing databases): H. Tazawa, T. Kunisada, Y. Hashimoto, S. Kagawa, Y. Urata, T. Ozaki
Study supervision: T. Sasaki, T. Kunisada, F. Uno, Y. Urata, T. Fujiwara

Acknowledgments

The authors thank Dr. Satoru Kyo (Kanazawa University) for providing the HOS and SaOS-2 cells and Tomoko Sueishi for her excellent technical support.

Grant Support

This study was supported by grants-in-aid from the Ministry of Education, Science, and Culture, Japan (T. Fujiwara) and grants from the Ministry of Health and Welfare, Japan (T. Fujiwara), and in part by the National Cancer Center Research and Development Fund (23-A-10) (T. Ozaki).

The costs of publication of this article were defrayed in part by the payment of page charges. This article must therefore be hereby marked *advertisement* in accordance with 18 U.S.C. Section 1734 solely to indicate this fact.

Received August 30, 2012; revised December 27, 2012; accepted December 29, 2012; published OnlineFirst January 11, 2013.

References

1. Ottaviani G, Jaffe N. The etiology of osteosarcoma. Cancer Treat Res 2009;152:15–32.
2. Damron TA, Ward WG, Stewart A. Osteosarcoma, chondrosarcoma, and Ewing's sarcoma: National Cancer Data Base Report. Clin Orthop Relat Res 2007;459:40–7.
3. Lewis IJ, Nooij MA, Whelan J, Sydes MR, Grimer R, Hogendoorn PC, et al. Improvement in histologic response but not survival in osteosarcoma patients treated with intensified chemotherapy: a randomized phase III trial of the European Osteosarcoma Intergroup. J Natl Cancer Inst 2007;99:112–28.
4. Bacci G, Longhi A, Versari M, Mercuri M, Briccoli A, Picci P. Prognostic factors for osteosarcoma of the extremity treated with neoadjuvant chemotherapy: 15-year experience in 789 patients treated at a single institution. Cancer 2006;106:1154–61.
5. Bielack SS, Kempf-Bielack B, Delling G, Exner GU, Flege S, Helmke K, et al. Prognostic factors in high-grade osteosarcoma of the extremities or trunk: an analysis of 1,702 patients treated on neoadjuvant cooperative osteosarcoma study group protocols. J Clin Oncol 2002; 20:776–90.
6. Siegel R, Naishadham D, Jemal A. Cancer statistics, 2012. CA Cancer J Clin 2012;62:10–29.
7. Buseman CM, Wright WE, Shay JW. Is telomerase a viable target in cancer? Mutat Res 2012;730:90–7.
8. Artandi SE, DePinho RA. Telomeres and telomerase in cancer. Carcinogenesis 2010;31:9–18.
9. Umehara N, Ozaki T, Sugihara S, Kunisada T, Morimoto Y, Kawai A, et al. Influence of telomerase activity on bone and soft tissue tumors. J Cancer Res Clin Oncol 2004;130:411–6.
10. Aogi K, Woodman A, Urquidi V, Mangham DC, Tarin D, Goodison S. Telomerase activity in soft-tissue and bone sarcomas. Clin Cancer Res 2000;6:4776–81.
11. Nakayama J, Tahara H, Tahara E, Saito M, Ito K, Nakamura H, et al. Telomerase activation by hTRT in human normal fibroblasts and hepatocellular carcinomas. Nat Genet 1998;18:65–8.
12. Kawashima T, Kagawa S, Kobayashi N, Shirakiya Y, Umeoka T, Teraishi F, et al. Telomerase-specific replication-selective virotherapy for human cancer. Clin Cancer Res 2004;10:285–92.
13. Nemunaitis J, Tong AW, Nemunaitis M, Senzer N, Phadke AP, Bedell C, et al. A phase I study of telomerase-specific replication competent oncolytic adenovirus (telomelysin) for various solid tumors. Mol Ther 2010;18:429–34.
14. Sasaki T, Tazawa H, Hasei J, Kunisada T, Yoshida A, Hashimoto Y, et al. Preclinical evaluation of telomerase-specific oncolytic virotherapy for human bone and soft tissue sarcomas. Clin Cancer Res 2011;17:1828–38.
15. Li G, Kawashima H, Ogose A, Ariizumi T, Xu Y, Hotta T, et al. Efficient virotherapy for osteosarcoma by telomerase-specific oncolytic adenovirus. J Cancer Res Clin Oncol 2011;137:1037–51.
16. Vousden KH, Prives C. Blinded by the light: the growing complexity of p53. Cell 2009;137:413–31.
17. Fujiwara K, Daido S, Yamamoto A, Kobayashi R, Yokoyama T, Aoki H, et al. Pivotal role of the cyclin-dependent kinase inhibitor p21WAF1/CIP1 in apoptosis and autophagy. J Biol Chem 2008;283:388–97.
18. Gorospe M, Cirielli C, Wang X, Seth P, Capogrossi MC, Holbrook NJ. p21(Waf1/Cip1) protects against p53-mediated apoptosis of human melanoma cells. Oncogene 1997;14:929–35.
19. Blagosklonny MV, el-Deiry WS. In vitro evaluation of a p53-expressing adenovirus as an anti-cancer drug. Int J Cancer 1996;67:386–92.
20. Zeng Y, Prabhu N, Meng R, Eldeiry W. Adenovirus-mediated p53 gene therapy in nasopharyngeal cancer. Int J Oncol 1997;11:221–6.
21. Clayman GL, el-Naggar AK, Lippman SM, Henderson YC, Frederick M, Merritt JA, et al. Adenovirus-mediated p53 gene transfer in patients with advanced recurrent head and neck squamous cell carcinoma. J Clin Oncol 1998;16:2221–32.
22. Swisher SG, Roth JA, Nemunaitis J, Lawrence DD, Kemp BL, Carrasco CH, et al. Adenovirus-mediated p53 gene transfer in advanced non-small-cell lung cancer. J Natl Cancer Inst 1999;91:763–71.
23. Shimada H, Matsubara H, Shiratori T, Shimizu T, Miyazaki S, Okazumi S, et al. Phase I/II adenoviral p53 gene therapy for chemoradiation resistant advanced esophageal squamous cell carcinoma. Cancer Sci 2006;97:554–61.
24. Fujiwara T, Tanaka N, Kanazawa S, Ohtani S, Saijo Y, Nukiwa T, et al. Multicenter phase I study of repeated intratumoral delivery of adenoviral p53 in patients with advanced non-small-cell lung cancer. J Clin Oncol 2006;24:1689–99.
25. Sakai R, Kagawa S, Yamasaki Y, Kojima T, Uno F, Hashimoto Y, et al. Preclinical evaluation of differentially targeting dual virotherapy for human solid cancer. Mol Cancer Ther 2010;9:1884–93.
26. Yamasaki Y, Tazawa H, Hashimoto Y, Kojima T, Kuroda S, Yano S, et al. A novel apoptotic mechanism of genetically engineered adenovirus-mediated tumour-specific p53 overexpression through E1A-dependent p21 and MDM2 suppression. Eur J Cancer 2012;48: 2282–91.
27. Hashimoto Y, Watanabe Y, Shirakiya Y, Uno F, Kagawa S, Kawamura H, et al. Establishment of biological and pharmacokinetic assays of telomerase-specific replication-selective adenovirus. Cancer Sci 2008;99:385–90.
28. Bagchi S, Raychaudhuri P, Nevins JR. Adenovirus E1A proteins can dissociate heteromeric complexes involving the E2F transcription factor: a novel mechanism for E1A trans-activation. Cell 1990;62: 659–69.
29. Emmrich S, Putzer BM. Checks and balances: E2F-microRNA crosstalk in cancer control. Cell Cycle 2010;9:2555–67.
30. Petrocca F, Vecchione A, Croce CM. Emerging role of miR-106b-25/miR-17-92 clusters in the control of transforming growth factor beta signaling. Cancer Res 2008;68:8191–4.
31. Tazawa H, Yano S, Yoshida R, Yamasaki Y, Sasaki T, Hashimoto Y, et al. Genetically engineered oncolytic adenovirus induces autophagic cell death through an E2F1-microRNA-7-epidermal growth factor receptor axis. Int J Cancer 2012;131:2939–50.
32. Crighton D, Wilkinson S, O'Prey J, Syed N, Smith P, Harrison PR, et al. DRAM, a p53-induced modulator of autophagy, is critical for apoptosis. Cell 2006;126:121–34.
33. Liu TC, Galanis E, Kirn D. Clinical trial results with oncolytic virotherapy: a century of promise, a decade of progress. Nat Clin Pract Oncol 2007;4:101–17.
34. van Beusechem VW, van den Doel PB, Grill J, Pinedo HM, Gerritsen WR. Conditionally replicative adenovirus expressing p53 exhibits enhanced oncolytic potency. Cancer Res 2002;62:6165–71.
35. Idogawa M, Sasaki Y, Suzuki H, Mita H, Imai K, Shinomura Y, et al. A single recombinant adenovirus expressing p53 and p21-targeting artificial microRNAs efficiently induces apoptosis in human cancer cells. Clin Cancer Res 2009;15:3725–32.
36. Chattopadhyay D, Ghosh MK, Mal A, Harter ML. Inactivation of p21 by E1A leads to the induction of apoptosis in DNA-damaged cells. J Virol 2001;75:9844–56.
37. Polager S, Ginsberg D. p53 and E2f: partners in life and death. Nat Rev Cancer 2009;9:738–48.
38. Wu X, Levine AJ. p53 and E2F-1 cooperate to mediate apoptosis. Proc Natl Acad Sci U S A 1994;91:3602–6.
39. Itoshima T, Fujiwara T, Waku T, Shao J, Kataoka M, Yarbrough WG, et al. Induction of apoptosis in human esophageal cancer cells by sequential transfer of the wild-type p53 and E2F-1 genes: involvement of p53 accumulation via ARF-mediated MDM2 down-regulation. Clin Cancer Res 2000;6:2851–9.
40. Tian X, Chen Y, Hu W, Wu M. E2F1 inhibits MDM2 expression in a p53-dependent manner. Cell Signal 2011;23:193–200.
41. Suh SS, Yoo JY, Nuovo GJ, Jeon YJ, Kim S, Lee TJ, et al. MicroRNAs/TP53 feedback circuitry in glioblastoma multiforme. Proc Natl Acad Sci U S A 2012;109:5316–21.
42. Huang S, Benavente S, Armstrong EA, Li C, Wheeler DL, Harari PM. p53 modulates acquired resistance to EGFR inhibitors and radiation. Cancer Res 2011;71:7071–9.
43. Salvatori L, Caporuscio F, Coroniti G, Starace G, Frati L, Russo MA, et al. Down-regulation of epidermal growth factor receptor induced by estrogens and phytoestrogens promotes the differentiation of U2OS human osteosarcoma cells. J Cell Physiol 2009;220: 35–44.

44. Dass CR, Choong PF. Zoledronic acid inhibits osteosarcoma growth in an orthotopic model. Mol Cancer Ther 2007;6:3263–70.
45. Labrinidis A, Hay S, Liapis V, Ponomarev V, Findlay DM, Evdokiou A. Zoledronic acid inhibits both the osteolytic and osteoblastic components of osteosarcoma lesions in a mouse model. Clin Cancer Res 2009;15:3451–61.
46. Ternovoi VV, Curiel DT, Smith BF, Siegal GP. Adenovirus-mediated p53 tumor suppressor gene therapy of osteosarcoma. Lab Invest 2006;86:748–66.
47. Hellwinkel OJ, Muller J, Pollmann A, Kabisch H. Osteosarcoma cell lines display variable individual reactions on wildtype p53 and Rb tumour-suppressor transgenes. J Gene Med 2005;7:407–19.
48. Ganjavi H, Gee M, Narendran A, Parkinson N, Krishnamoorthy M, Freedman MH, et al. Adenovirus-mediated p53 gene therapy in osteosarcoma cell lines: sensitization to cisplatin and doxorubicin. Cancer Gene Ther 2006;13:415–9.
49. Lambert LA, Qiao N, Hunt KK, Lambert DH, Mills GB, Meijer L, et al. Autophagy: a novel mechanism of synergistic cytotoxicity between doxorubicin and roscovitine in a sarcoma model. Cancer Res 2008;68:7966–74.
50. Su C, Cao H, Tan S, Huang Y, Jia X, Jiang L, et al. Toxicology profiles of a novel p53-armed replication-competent oncolytic adenovirus in rodents, felids, and nonhuman primates. Toxicol Sci 2008;106: 242–50.

IJC
International Journal of Cancer

A novel synergistic effect of iron depletion on antiangiogenic cancer therapy

Toshiaki Ohara[1], Kazuhiro Noma[1], Shinichi Urano[1], Shinichiro Watanabe[1], Seishi Nishitani[1], Yasuko Tomono[2], Fumiaki Kimura[3], Shunsuke Kagawa[1], Yasuhiro Shirakawa[1] and Toshiyoshi Fujiwara[1]

[1] Department of Gastroenterological Surgery, Okayama University Graduate School of Medicine, Dentistry and Pharmaceutical Sciences, Okayama, Japan
[2] Shigei Medical Research Institute, Okayama, Japan
[3] Department of Internal Medicine, Tamano City Hospital, Okayama, Japan

Iron is an essential element for both normal and cancer cells in humans. Treatment to reduce iron levels has been shown to suppress tumor growth *in vivo*. However, iron depletion monotherapy by iron decreased treatment has not been thought to be superior to ordinary chemotherapy and is not part of the standard therapeutic strategy for the treatment of cancer. Iron depletion is also known to reduce serum hemoglobin and oxygen supply to the tissue, which indicates that iron depletion may induce angiogenesis. Therefore, we hypothesized that iron depletion with antiangiogenic therapy can have a novel therapeutic effect in the treatment of cancer. Human nonsmall cell carcinoma cell lines A549 and H1299 were used in our study. An iron-deficient diet and an iron chelator were used to simulate an iron-depleted condition. The antitumor effects of iron depletion and antiangiogenic therapy were determined on A549 xenograft mice. The iron-depleted condition produced by an iron-deficient diet suppressed tumor growth. Tumor tissue from the iron-deficient diet group showed that cancer cell proliferation was suppressed and hypoxia was induced. Microvessel density of this group was increased which suggested that the iron-depleted condition induced angiogenesis. Bevacizumab administration had a synergetic effect on inhibiting the tumor growth on Day 39. An iron-depleted condition inhibited cancer cell proliferation and reciprocally induced angiogenesis. Bevacizumab synergistically enhanced the iron-depleted antitumor effect. Treatment to deplete iron levels combined with anti-angiogenic therapy could induce a novel therapeutic effect in the treatment of cancer.

Introduction

Chemotherapy is continually evolving and various anticancer drugs have been produced during the past decades. Recently, therapies targeting molecules in cancer cells have been developed and used in the clinical setting. Moreover, new drugs targeting the tumor stroma have been developed. Bevacizumab, an antibody against vascular endothelial growth factor (VEGF), is the first tumor stroma molecular-targeting drug.[1] Many kinds of cancer cells are known to become hypoxic during progression of the tumor. However, the cells survive with angiogenesis through activation of VEGF signaling *via* hypoxia-induced factor 1α (HIF-1α).[2] Bevacizumab has been used to treat many different cancers all over the world and some clinical studies revealed that bevacizumab prolonged survival.[3–5]

Iron metabolism and its relationship with cancer cells have been studied for a long time. Iron is an essential element for both human normal and cancer cells. Iron overload is known to induce some kinds of cancer, which suggests that the prevention of iron overload may become a therapeutic strategy for cancer prevention.[6,7] In fact, reduction of serum iron with phlebotomy lowered the risk of developing hepatocellular carcinoma in patients with chronic hepatitis C.[8] Iron-depletion treatment is also known to suppress tumor growth *in vivo*.[9] However, iron-depletion monotherapy has generally been thought to not be superior to ordinary chemotherapy and a standard therapeutic strategy in the treatment of cancer.

In human biology, iron depletion was known to reduce serum hemoglobin and oxygen supply to the tissue.[10,11] Therefore, cancer cells could respond to iron depletion and induce angiogenesis to compensate for the reduced oxygen supply. Subsequently, their iron-decreased status could make the cancer cell more dependent on angiogenesis so that the effectiveness of antiangiogenic therapy would be increased in an iron-depleted condition.

Key words: angiogenesis, bevacizumab, chelator, iron
Abbreviations: CD31: cluster of differentiation 31; HIF-1α: hypoxia-induced factor 1α; MVD: microvessel density; NSCLC: non-small cell lung cancer; RECIST: response evaluation criteria in solid tumors; TfR-1: transferrin receptor 1; VEGF: vascular endothelial factor
Additional Supporting Information may be found in the online version of this article.
Grant sponsors: Grants-in-Aid from the Ministry of Education, Science, and Culture, Japan, The Ministry of Health and Welfare, Japan
DOI: 10.1002/ijc.27943
History: Received 15 Jun 2012; Accepted 17 Oct 2012; Online 15 Nov 2012
Correspondence to: Toshiyoshi Fujiwara, Department of Gastroenterological Surgery, Okayama University Graduate School of Medicine, Dentistry and Pharmaceutical Sciences, 2-5-1 Shikata-cho, Kita-ku, Okayama 700-8558, Japan, Tel: +81-86-235-7257, Fax: +81-86-221-8775, E-mail: toshi_f@md.okayama-u.ac.jp

What's new?
Withholding iron from tissues reduces their access to oxygen, and can suppress tumor cell proliferation. If reducing the availability of iron could weaken tumors, making them less able to withstand traditional therapies, that would be an inexpensive and simple way to boost outcomes. The current study investigated whether limiting the iron supply enhanced the effectiveness of anti-angiogenic therapy. In mice fed an iron-deficient diet, tumor growth slowed. When an iron-chelating agent was used in conjunction with the anti-angiogenesis drug bevacizumab, the anti-tumor treatment worked significantly better, suggesting that iron reduction could be a very promising way to enhance cancer therapy.

In our study, we investigated whether iron-depletion and anti-angiogenic therapy can have a novel therapeutic effect for the treatment of cancer.

Material and Methods

Cell lines and cultures

The human nonsmall cell lung cancer (NSCLC) cell lines A549 and H1299 were used in our study. A549 was cultured in Dulbecco's modified eagle medium (DMEM, Sigma-Aldrich, St. Louis, MO) and H1299 was cultured in RPMI1640 medium (Sigma-Aldrich) at 37°C in humidified air with 5% CO_2. Each medium was supplemented with 10% fetal calf serum (FCS, Hyclone, Logan, UT), 100 units/mL penicillin, and 100 mg/mL streptomycin (Sigma-Aldrich).

Reagents

Bevacizumab, commercialized as AVASTIN™ by Roche (Basel, Switzerland), was purchased from Chugai Pharmaceutical (Tokyo, Japan). Bevacizumab was diluted to the final concentration of 5 mg/kg with 0.9% sodium chloride before use *in vivo*. Deferasirox, commercialized as EXJADE™ was purchased from Novartis Pharma (Tokyo, Japan).

Cell viability assay

The proliferation of A549 and H1299 cells was evaluated using a sulfonated tetrazolium salt (WST-1). The cells were plated at a density of 1×10^3 cells/well in 96-well micro plates, in 10% FCS containing each mediu, and incubated at 37°C in a humidified atmosphere of 5% CO_2. Twenty-four hours after each treatment, the cells were incubated with 10 μL/well of WST-1/PBS solution (Roche) for 3 hr under the same conditions as indicated above. The absorbance of the samples was measured at 450 nm using a microplate reader with a background control as the blank. The cell viability ratio was expressed as a percentage of the control.

Cell-cycle analysis by flow cytometry

For the cell-cycle analysis, cancer cells were plated in six-well tissue culture plates and treated with different concentrations of deferasirox (0, 1, 10,100 or 1,000 μM). After 24 hr, the cells were harvested and stained with 20 mg/mL propidium iodide. The DNA content was analyzed with a fluorescence-activated cell sorter (FACScan, Becton Dickinson, Franklin Lakes, NJ) using Cell Quest software (BD Biosciences, San Jose, CA).

Western blotting

Whole-cell lysates and nuclear protein were extracted using M-PER buffer (Thermo Fisher Scientific, Rockford, IL) and NE-PER buffer (Thermo Fisher Scientific), respectively. Total protein extraction and nuclear protein from homogenized A549 xenograft tumor tissue samples were extracted using T-PER buffer (Thermo Fisher Scientific) and NE-PER buffer (Thermo Fisher Scientific). The collected supernatants were subjected to protein concentration and equal amounts of protein were electrophoresed under reducing conditions in gradient polyacrylamide gels (ATTO, Tokyo, Japan) and were then transferred onto polyvinylidene difluoride filter membranes (Millipore, Billerica, MA). The membranes were incubated with primary antibodies at 4°C overnight, followed by incubation with secondary antibodies at room temperature for 1 hr. An Amersham chemiluminescent ECL Plus Western Blotting Detection system (GE Healthcare, Piscataway, NJ) was used for signal detection. Western blotting materials were as follows: hydroxy-HIF-1α (Pro564) (D43B5) was obtained from Cell Signaling Technology (Beverly, MA); cyclin D1 was obtained from Santa Cruz Biotechnology (Santa Cruz, CA); β-actin was obtained from Sigma-Aldrich; horseradish peroxidase-conjugated rabbit anti-mouse IgG was obtained from Dako Cytomation (Glostrup, Denmark); and goat anti-rabbit IgG was obtained from American Qualex Antibodies (La Mirada, CA).

Histology and immunohistology

Surgically resected tissues from the A549 xenograft model were used for histological and immunohistochemical study. Paraffin sections were prepared from the 10% formalin-fixed tumors and stained with hematoxylin/eosin and Prussian blue. Prussian blue staining was performed by incubating fixed tissue in a mixture of 2% potassium ferrocyanide and 1% HCl for 30 min. Glass slides were rinsed in distilled water and counterstained with Nuclear Fast Red for 5 min. Immunohistochemical procedures were followed as described previously.[12] Deparaffinized tissue sections were immersed in methanol containing 3% hydrogen peroxide to block endogenous peroxide activity. An autoclave pretreatment in citrate buffer was done for antigen retrieval. A Ki-67 staining kit (Dako) and CD31 (endothelial cell adhesion molecule-1) rabbit monoclonal antibody (Santa Cruz Biotechnology) were used. After incubation with a blocking buffer, the sections were treated with Ki-67 and CD31 antibodies for 1 hr at room temperature followed by immunobridging with Avidin DH-biotinylated

Table 1. Content of control and iron-deficient diets

	Control diet	Iron-deficient diet
g/kg diet		
Corn starch	610	610
Casein	220	220
Cellulose	50	50
Soybean oil	40	40
Vitamin mixture	10	10
Mineral mixture		
Potassium	17.3	17.3
Phosphorus	15	15
Calcium	13.55	13.55
Magnesium	8	8
Corn starch	8	9.9
Sodium	6	6
Iron	1.9	
Manganese	0.154	0.154
Zinc	0.06	0.06
Iodine	0.0154	0.0154
Copper	0.0126	0.0126
Chloride	0.004	0.004

horseradish peroxide complex (Nichirei, Tokyo, Japan). Signal detection was done for 2–5 min using a solution of 3,3′-diaminobenzidine tetrahydrochloride in 50 mmol/L Tris-HCl (pH = 7.5) containing 0.001% hydrogen peroxide. The sections were counterstained with Mayer's hematoxylin for 6 hr at room temperature followed by immunobridging with Avidin DH-biotinylated horseradish peroxide complex (Nichirei). Ki-67 labeling index was calculated as the average percentage of Ki-67-positive nuclei in three high-power fields (HPFs).

Hypoxia assay

A Hypoxyprobe-1 kit (Chemicon International, Temecula, CA) was used to investigate tumor hypoxia. Mice were injected intraperitoneally (ip) with Hypoxyprobe TM-1 [pimonidazole hydrochloride 60 mg/kg] 45 min before tumor collection.[13,14] The collected tumor sections were incubated for 1 h with the Hypoxyprobe-1 primary antibody supplied with the kit.

Micro vessel density

Angiogenesis activity was determined to count microvessel density. CD31-immunostained sections were used in the previous report.[15] The highest density of blood vessels (hot spots) was selected at a low-power field and the number of blood vessels was counted per 0.20 mm^2 in five separate hot spots at a HPF.[16] All sections were scored independently by two individual experienced microscopists and no significant differences were observed between scorers.

Table 2. Blood analysis results of the normal and iron-deficient diet groups

	Fe (+)	Fe (−)	*p*-Value
RBC ($\times 10^4$)	891 ± 46	802 ± 43	0.029
WBC	4,425 ± 1,258	3,575 ± 150	0.228
Hb	14.9 ± 0.7	11.4 ± 0.6	0.001
HCT	46.2 ± 3.7	38.5 ± 3.8	0.027
MCV	52.0 ± 2.0	48.5 ± 2.4	0.065
MCHC	30.3 ± 1.3	29.8 ± 1.3	0.594
Fe	222.3 ± 20.1	115.3 ± 43.3	0.004
Ferritin	255.0 ± 108.6	113.8 ± 24.9	0.044

VEGF ELISA assay

To evaluate the supernatant VEGF secreted by A549 and H1299 cells, we used a VEGF enzyme-linked immunosorbent assay (ELISA) kit (R&D Systems, Minneapolis, MN). The cancer cells were plated in six-well tissue culture plates and were treated with different concentrations of deferasirox (0, 1, 10, 100 or 1,000 μM). After a 24-hr treatment, the supernatant and cells were harvested and VEGF content was assayed by ELISA according to the protocol provided by the manufacturer. The results were normalized to the concentration of total protein extraction per plate. Data were presented as mean ± SD from three independent experiments.

Animal experiments

The animal experimental protocol was approved by the Ethics Review Committee for Animal Experimentation of Okayama University, Okayama, Japan. All of the mice and their diets (normal and iron deficient) were purchased from Clea (Tokyo, Japan) (Table 1). The 6-week-old male BALB/c nu/nu mice were randomized into two groups of eight mice each; (*i*) normal diet as a control and (*ii*) iron-deficient diet. After 3 weeks, A549 subcutaneous xenografts were produced on the backs of mice by injecting 3×10^6 cells mixed with Matrigel (BD Biosciences) at a 1:1 ratio.[17,18] Water was provided and the mice were allowed to drink freely. Tumor volume was measured weekly (length × $width^2/2$). For the bevacizumab administration study, 6-week-old male BALB/c nu/nu mice were randomized into two groups of 20 mice each as above. After 3 weeks, A549 subcutaneous xenografts were produced in the same way. After a week, the mice in each diet group were randomized into two groups of four mice each (*i*) bevacizumab (5 mg/kg twice/week for 5 weeks), (*ii*) saline alone as a control.[15] The drug was administered ip and tumor volume measured twice a week. Both diets (normal and iron deficient) and water were provided *ad libitum*.

Statistical analysis

A Student's *t*-test was used to compare data between the two groups. Data represent the mean ± SD; $p < 0.05$ was considered statistically significant.

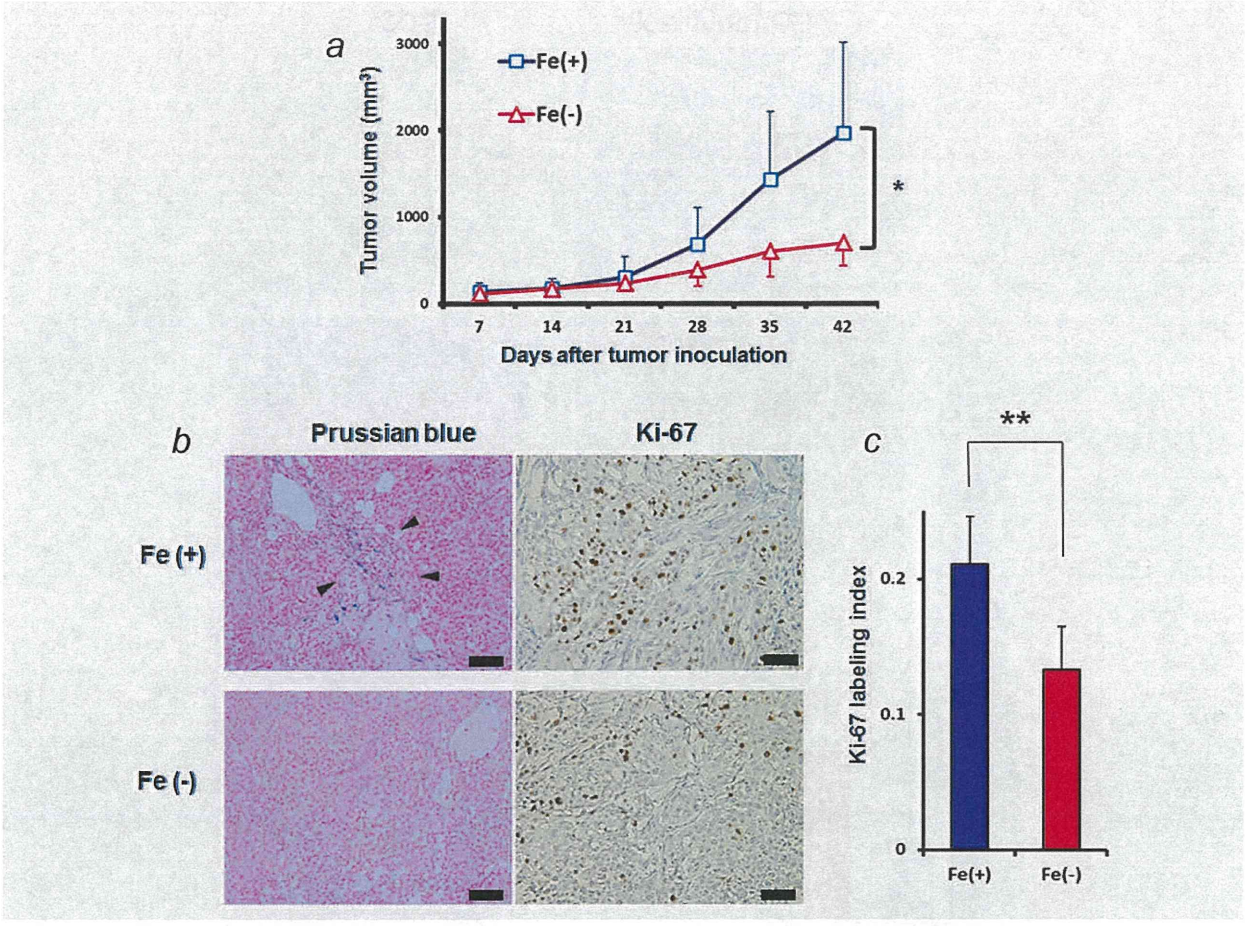

Figure 1. Iron depletion suppressed tumor growth *in vivo*. (*a*) An iron-deficient diet was started 3 weeks before inoculating A549 cells on the backs of mice. The iron-deficient diet was continuously fed until the end of the study. Tumor volume was measured as a cube (length × width × height) and was tracked up to 6 weeks. Tumor growth was suppressed in the iron-deficient diet group. Tumor growth was expressed as mean tumor volume ± SD. Statistical significance (*) was determined as $p < 0.01$. (*b*) Prussian blue and Ki-67 staining showed the positive spot area and proliferating cells were reduced in the iron-depleted condition. Scale bars: 50 mm. (*c*) Ki-67 labeling index was decreased in iron-depleted condition. Data are means ± SD. Statistical significance (**) was determined as $p < 0.05$.

Results

Iron-deficient diet produced iron-depleted mice

We first confirmed that the iron-deficient diet resulted in an iron-depleted mouse model. The 6-week-old male BALB/c nu/nu mice were randomized into two groups of eight mice each. Blood sampling was performed after 3 weeks. The iron-deficient diet reduced serum iron levels (Table 2). To confirm iron deficiency histologically, Prussian blue staining was done using surgically resected murine spleens. Although the positive blue spots were diffusely recognized in the normal diet group, no positive blue spot was recognized in the iron-deficient diet group (Supporting Information Fig. 1). A reduction of iron in the reticuloendothelial system proves that the iron-deficient diet reduced serum iron levels.

Iron depletion suppressed tumor growth

We investigated the tumor growth under an iron-depleted condition. A549 subcutaneous xenografts were produced on the backs of mice after 3 weeks of an iron-deficient diet and tumor size was measured once a week. Tumor growth was suppressed in the iron-deficient diet group (tumor volume: normal diet *vs.* iron-deficient diet = 1,375.9 ± 688.4 *vs.* 497.0 ± 192.2 mm^3; $p = 0.0037$) (Fig. 1*a*). There were no mice that died and no significant side effects were observed during the experiment. Moreover, diet intake and body weight were not significantly different between normal diet group and iron-deficient diet group (Supporting Information Fig. S2).

Iron depletion reduced iron levels in tumor tissue and suppressed cancer cell proliferation

To identify the differences in tumor progression in an iron-depleted condition, we performed histological and immunohistological examinations (Fig. 1*b*). As shown above, an iron-deficient diet reduced the serum and tumor tissue iron levels. Interestingly, there was only difference of positive spot area in stroma tissue of the tumor. Proliferating cells (G1, S, G2 and M cycling stages of cell division) were stained

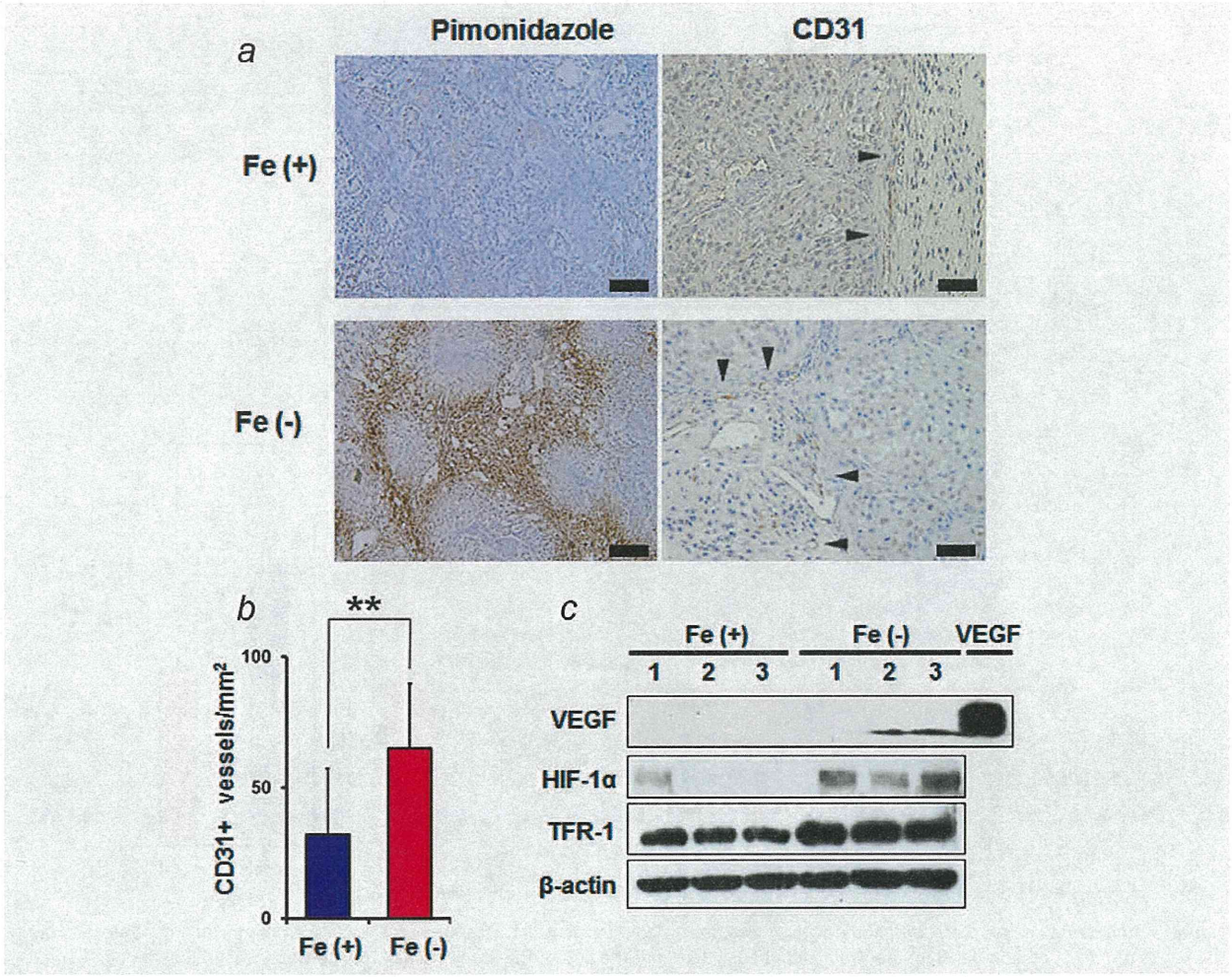

Figure 2. Iron depletion reciprocally induced angiogenesis *via* upregulation of HIF-1α. (*a*) Tumor tissues obtained as described in the legend to Figure 1 were analyzed for angiogenesis. Pimonidazole and CD-31 staining showed that positive spot area and positive stained vessels were increased in the iron-depleted condition. Scale bars: 50 mm. (*b*) MVD is increased in the iron-depleted condition. Data are means ± SD. Statistical significance (**) was determined as $p < 0.05$. (*c*) Western blot analysis of tumor-homogenized samples showed that VEGF and TfR-1 were upregulated in the iron-depleted condition. Similarly, HIF-1α was also upregulated at the nucleus protein level. Each tumor sample was obtained from three individual mice.

positive; G0 cycling stage cells were excluded. The Ki-67 labeling index revealed that an iron-deficient diet suppressed cancer cell proliferation compared to the normal diet group (Ki-67 labeling index: normal diet *vs.* iron-deficient diet = 0.211 ± 0.035 *vs.* 0.133 ± 0.032; $p = 0.0459$). Prussian blue staining was almost negative in the tissue in iron-deficient group.

Iron depletion followed by hypoxia and angiogenesis

We hypothesized that iron depletion induced a reduction of serum hemoglobin and tissue hypoxia. Iron depletion also upregulates angiogenesis in the tumor. To test these hypotheses, we investigated pimonidazole and CD-31 staining (Fig. 2*a*). Tumor hypoxia was increased in the group fed an iron-deficient diet. CD-31 staining was performed to investigate whether iron depletion induced angiogenesis. Microvessel density (MVD) was calculated to count CD-31-positive vessels (Fig. 2*b*). CD-31-positive vessels were increased in an iron-depleted condition. The MVD of the iron-deficient diet group was higher than that of the normal diet group (MVD: normal diet *vs.* iron-deficient diet = 32.02 ± 25.24 *vs.* 64.96 ± 24.71; $p = 0.045439$). This result suggested that iron depletion induced angiogenesis via hypoxia.

Angiogenesis was induced by iron depletion via HIF-1α upregulation

To identify the mechanism by which iron depletion induced angiogenesis *via* hypoxia, a Western blot analysis was performed using homogenized tissue samples. The expression of transferrin receptor 1 (TfR-1) was determined to confirm the effect of iron depletion in tumor tissue samples. As TfR-1

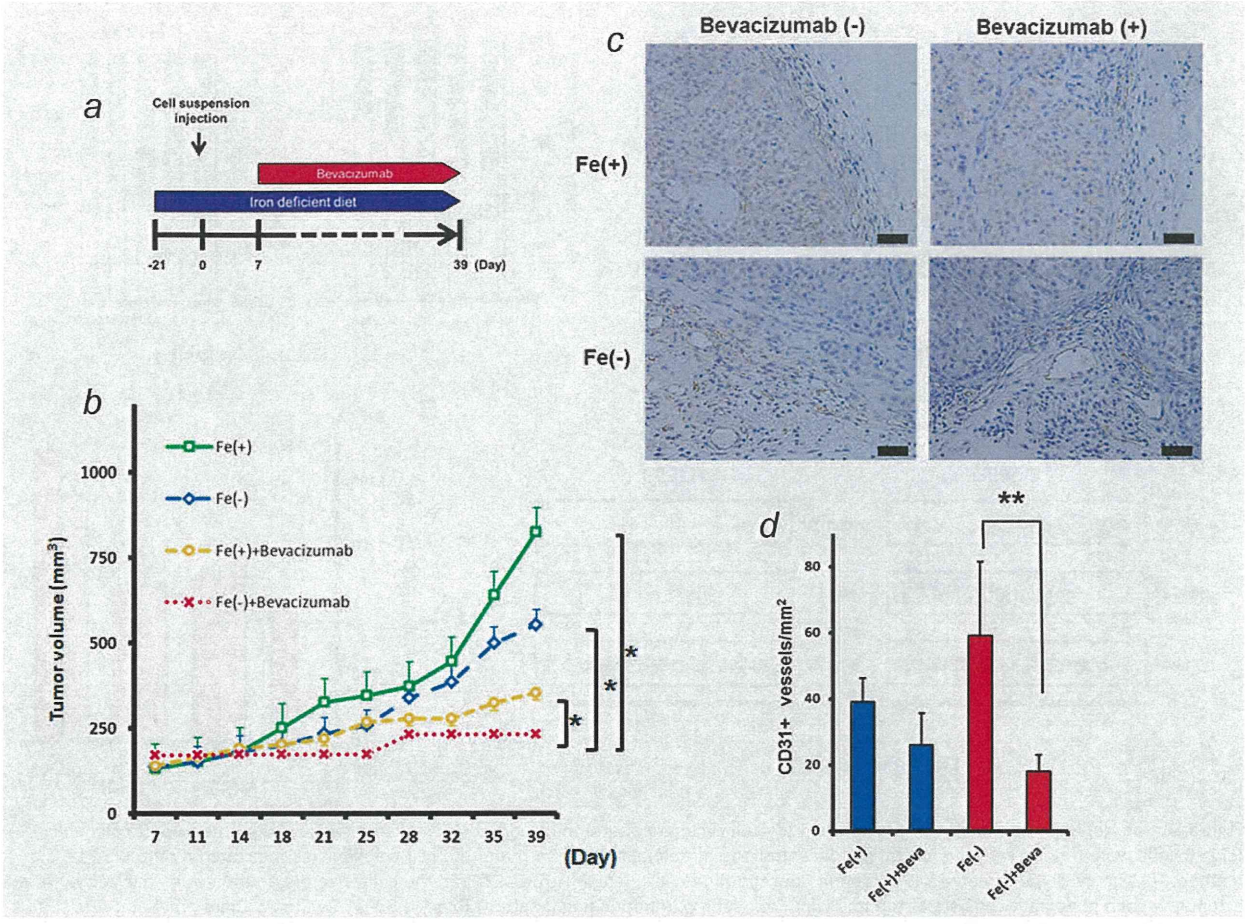

Figure 3. Bevacizumab synergistically suppressed tumor growth in an iron-depleted condition. (*a*) An iron-deficient diet was started 3 weeks before inoculating A549 cells on the backs of mice (day 21). The iron-deficient diet was continuously fed until the end of the study. (*b*) Bevacizumab (5 mg/kg) or saline as a control was administered ip twice/week. Tumor volume was measured as a cube (length × width × height) and was tracked up to 39 days. Five mice were used for each group. Tumor growth was expressed as mean tumor volume ± SD. Statistical significance (*) was determined as $p < 0.01$. Tumor growth was significantly inhibited in the combination group as compared to the control, bevacizumab or Fe (–) groups. (*c*) CD-31 staining revealed that positively stained vessels were increased in the iron-depleted condition. Scale bars: 50 mm. (*d*) Bevacizumab decreased MVD in both normal diet group and iron-deficient diet group.

expression changes based on the serum iron level, a decrease in serum iron levels increases TfR-1 expression.[19] Whole-cell lysate from homogenized tissue samples showed TfR-1 was upregulated in the iron-deficient diet group (Fig. 2*c*). Subsequently, the expression status of HIF-1α in nuclei was determined. HIF-1α is known to play a critical role in angiogenesis *via* hypoxia.[2,20] Western blot analysis of an extraction from nuclei showed the expression of HIF-1α in the iron-deficient diet group was higher than that of the normal group (Fig. 2*c*). This result suggested that iron depletion induced hypoxia *via* HIF-1α, which caused angiogenesis.

Bevacizumab synergistically suppressed tumor growth by inhibiting upregulated angiogenesis

As shown above, we found that iron depletion was followed by hypoxia and angiogenesis. Thus, an antiangiogenic therapeutic agent (bevacizumab) was predicted to have a synergetic effect on suppressing tumor growth in an iron-depleted condition. Bevacizumab was administrated ip 5 mg/kg twice a week to mice with subcutaneous tumors fed either an iron-deficient or a normal diet. This dose and schedule were cited in the previous reports.[21,22] Bevacizumab had a synergistic effect on inhibiting tumor growth on Day 39 (tumor volume: normal diet [857.6 ± 129.0 cm^3], iron-deficient diet [401.8 ± 126.6 cm^3], normal diet + bevacizumab [221.6 ± 63.8 cm^3], iron-deficient diet + bevacizumab [61.0 ± 27.5 cm^3]) (Figs. 3*a* and 3*b*). To calculate MVD, CD-31 staining was performed (Fig. 3*c*). We could confirmed that bevacizumab inhibited angiogenesis in spite of induction by iron depletion condition (MVD: normal diet [39 ± 7.3], iron-deficient diet [59 ± 22.4], normal diet + bevacizumab [26 ± 9.7], iron-